Two-dimensional superconductivity at the (111)LaAlO$_3$/SrTiO$_3$ interface

A. M. R. V. L. Monteiro,[*] D. J. Groenendijk, I. Groen, J. de Bruijckere, R. Gaudenzi, H. S. J. van der Zant, and A. D. Caviglia[†]

Kavli Institute of Nanoscience, Delft University of Technology, P.O. Box 5046, 2600 GA Delft, The Netherlands

We report on the discovery and transport study of the superconducting ground state present at the (111)LaAlO$_3$/SrTiO$_3$ (LAO/STO) interface. The superconducting transition is consistent with a Berezinskii-Kosterlitz-Thouless transition and its two-dimensional nature is further corroborated by the anisotropy of the critical magnetic field, as calculated by Tinkham. The estimated superconducting layer thickness and coherence length are 10 and 60 nm, respectively. The results of this work provide insight to clarify the microscopic details of superconductivity in LAO/STO interfaces, in particular in what concerns the link with orbital symmetry.

Transition metal oxide interfaces host a rich spectrum of functional properties which are not present in their parent bulk constituents [1]. Following the groundbreaking discovery of a high-mobility two-dimensional electron system (2DES) at the interface between the two wide band-gap insulators LaAlO$_3$ (LAO) and SrTiO$_3$ (STO) [2], a growing body of research efforts have brought to light many of its interesting properties. The system features a gate tunable metal-to-insulator transition [3,4], strong Rashba spin-orbit coupling [5], and superconductivity [6], possibly in coexistence with magnetism [7,8]. To date, the vast majority of research efforts have been directed toward the investigation of the (001)-oriented LAO/STO interface. However, it is well recognized that the direction of confinement plays a pivotal role in determining hierarchy of orbital symmetries and, consequently, in properties such as the spatial extension of the 2DES and the Rashba spin-orbit fields [9]. Recent work suggests that (111)-oriented ABO_3 perovskites are potentially suitable for the realization of topologically nontrivial phases [10], since along this direction a bilayer of B-site ions forms a honeycomb lattice. The 2DES at the (111)LAO/STO interface [11] is an interesting subject of investigation, combining a polar discontinuity at the interface with such a hexagonal lattice. Signatures of the sixfold symmetry related to the (111)STO orientation have recently been observed by angle-resolved photoemission spectroscopy (ARPES) [12,13] and magnetoresistance [14,15] measurements, making the system potentially suitable for exotic time-reversal symmetry breaking superconductivity [16]. Moreover, ARPES measurements at the surface of (111)STO have confirmed a distinct orbital ordering of the t_{2g} manifold [12], where all the bands are degenerate at the Γ point. This implies the absence of a Lifshitz point, considered to be at the origin of many physical properties at the (001)-oriented interface. In particular, the "optimal doping" for superconductivity was found to occur concomitantly with the Lifshitz transition [17]. Therefore, within this view, it is timely to investigate whether a 2D superconducting ground state arises at the (111) orientation.

The (111)LAO/STO interface under investigation was prepared by pulsed laser deposition. An LAO film with a thickness of 9 unit cells (u.c.) was epitaxially grown on a commercially available (111)STO substrate with Ti-rich surface. The film was deposited at 840 °C in an oxygen pressure of 6×10^{-5} mbar. The laser pulses were supplied by a KrF excimer source ($\lambda = 248$ nm) with an energy density of 1 J/cm^2 and a frequency of 1 Hz. The growth process was followed by an annealing step in order to refill oxygen vacancies. The chamber was filled with 300 mbar of oxygen and the sample temperature was kept at 600 °C for 1 h. The sample was then cooled down to room temperature at a rate of 10 °C/min in the same oxygen atmosphere. The growth process was monitored *in situ* using reflection high-energy electron diffraction (RHEED), which indicates a layer-by-layer growth mode as shown in Fig. 1(a). An atomic force microscope (AFM) topographic image of the surface after growth is shown in Fig. 1(b), where an atomically flat surface with step-and-terrace structure can be observed. The step height corresponds to the (111)STO interplanar distance (≈ 2.25 Å). Transport measurements were carried out in a Hall bar geometry, as shown in Fig. 1(c). The fabrication process relied on argon dry etching in order to define the channel and electron beam (e-beam) evaporation of metal contacts (for a detailed description, see Supplemental Material [18]). Hall bars were patterned along different in-plane orientations (0°, 30°, 60°, and 90°) in order to investigate possible anisotropies in the transport properties.

The temperature dependence of the sheet resistance (R) is shown in Fig. 2(a), evidencing a clear metallic behavior and absence of carrier localization down to 1.5 K. At this temperature the back gate voltage is swept to the maximum applied voltage (90 V) and back to 0 V. At variance with previous reports, we observed no hysteretic or anisotropic transport behavior attributed to the presence of oxygen vacancies [19]. All further measurements presented in this work are shown for one Hall bar recorded at a fixed back gate voltage of 30 V. The detailed investigation of the evolution of the transport properties with electrostatic doping shall be discussed elsewhere.

In the millikelvin regime, a superconducting transition with a critical temperature $T_c \approx 117$ mK is observed [Fig. 2(a)]. The value of T_c was defined as the temperature at which the resistance is 50% of its normal state value (R_n, measured at $T = 180$ mK). The width of the transition, defined between 20% and 80% of R_n, is $\Delta T_c = 17$ mK.

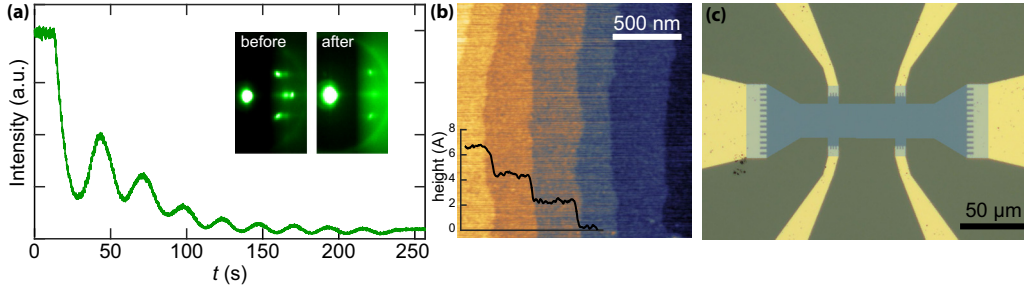---
[*]A.M.Monteiro@tudelft.nl
[†]A.Caviglia@tudelft.nl

FIG. 1. (a) RHEED intensity oscillations of the specular spot during the epitaxial growth of a 9 u.c. LaAlO$_3$ film on a (111)SrTiO$_3$ substrate. Inset: RHEED pattern before and after growth. (b) AFM topographic image of the surface after growth. Inset: height profile. (c) Optical image of a Hall bar. The channel is false-colored in blue.

For a 2D system, it is well established that superconductivity should exhibit a Berezinskii-Kosterlitz-Thouless (BKT) transition, at a characteristic temperature T_{BKT}. Below this temperature, vortex-antivortex pairs are formed. As the temperature increases and approaches T_{BKT}, a thermodynamic instability occurs and the vortex-antivortex pairs spontaneously unbind into free vortices. The resulting proliferation of free vortices destroys superconductivity, yielding a finite-resistance state. According to the BKT scenario, a strong non-Ohmic behavior in the $V(I)$ characteristics emerges near T_{BKT}, following a power-law behavior $V \propto I^{a(T)}$ with $a = 3$ at T_{BKT}.

In order to investigate the 2D character of superconductivity in the system, we measured the $V(I)$ characteristics of a 9 u.c. (111)LAO/STO interface as a function of temperature. The characteristics were recorded from 82 mK, where the samples are completely superconducting, up to the temperature at which the sample fully recovers to the normal state. As shown

in Fig. 2(b), there is a clear superconducting current plateau for the $V(I)$ curve at 82 mK. As the temperature is increased, the supercurrent plateau becomes progressively shorter, until it vanishes at approximately 127 mK. At this temperature, the $V(I)$ curve becomes completely linear. Concomitantly with the disappearance of the superconducting plateau, power-law type $V(I)$ curves emerge, indicating a BKT transition. In order to confirm this scenario, we plot the $V(I)$ characteristics on a logarithmic scale, as shown in Fig. 2(c). At sufficiently low current, the $V(I)$ characteristics display Ohmic behavior in the entire temperature range due to well-known finite size effects [20,21]. At higher current values, the $V(I)$ curves show a clear $V \propto I^{a(T)}$ power-law dependence, as indicated by the red lines. The black line corresponds to $V \propto I^3$. The exponents $a(T)$ are obtained by fitting all the characteristics and are plotted as a function of temperature in Fig. 2(d), revealing that $T_{BKT} \approx 91$ mK. At $T > T_{BKT}$, $V \propto I$ at low currents, transitioning to a strongly nonlinear behavior at higher currents and showing the characteristic rounding. In contrast, at $T < T_{BKT}$ the power-law behavior terminates abruptly with a voltage jump at a well defined current. It should be noted that the evolution of $a(T)$ does not display the characteristic discontinuous jump from $a(T_{BKT}^+) = 1$ to $a(T_{BKT}^-) = 3$, but rather transitions smoothly from 1 to 3 over a range of several millikelvin. This behavior, also observed in (001)- and (110)-oriented interfaces [6,22], stems from inhomogeneities in the local superconducting properties of the system (such as inhomogeneous superfluid density [23] or structural twin domains of the STO substrate [24]) which smear the universal jump [25].

For a quantitative estimation of both the superconducting coherence length (ξ) and the layer thickness (d), we carried out an analysis based on the Landau-Ginzburg formalism. To this purpose, a quantitative criterion was chosen in order to determine the out-of-plane ($B_c^\perp$) and in-plane ($B_c^\parallel$) critical magnetic fields. At each temperature, $V(I)$ characteristics are recorded for increasing values of applied magnetic field. As shown in the Supplemental Material, for small applied magnetic fields the values of $dV/dI_{I=0\,\text{nA}}$ are zero at low currents, corresponding to the superconducting state. As the current rises, dV/dI increases until a saturating value, $dV/dI_{I=200\,\text{nA}}$, which corresponds to the normal state resistance. For larger applied magnetic fields, $dV/dI_{I=0\,\text{nA}}$ is nonzero, and its value increases with the magnitude of the applied magnetic field.
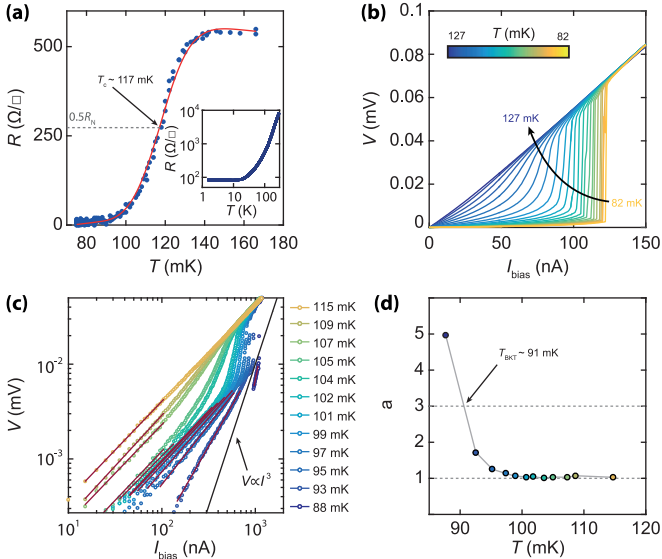

FIG. 2. (a) Sheet resistance (R) as a function of temperature (T) in the millikelvin regime with an applied back gate voltage of 30 V. Inset: $R(T)$ in the high-temperature range down to 1.5 K. (b) $V(I)$ characteristics measured at different temperatures. (c) Selected curves of panel (b) plotted in logarithmic scale. The red lines are fits of the data along the transition. The black line corresponds to $V \propto I^3$. (d) Temperature dependence of the power-law exponent $a(T)$ as determined from the fits shown in (c).
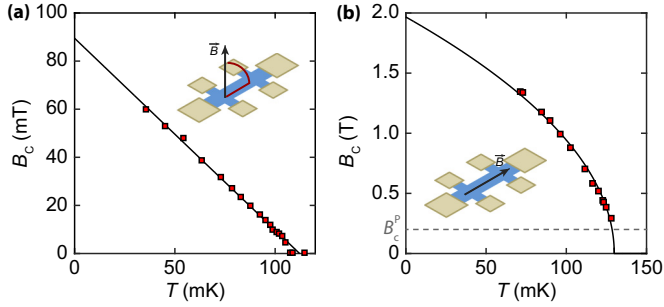
FIG. 3. (a) Out-of-plane and (b) in-plane critical magnetic field as a function of temperature. Dashed line: Pauli-limiting field.

We define the critical magnetic field as the value at which $dV/dI_{I=0\ \text{nA}}$ reaches 50% of the normal state resistance, i.e., $(dV/dI)_{I=0\ \text{nA}}/(dV/dI)_{I=200\ \text{nA}} = 0.5$.

We track the temperature evolution of the critical magnetic field for the out-of-plane and in-plane orientations, which are shown in Figs. 3(a) and 3(b), respectively. The black lines represent a fit to the expected dependence for a 2D superconductor, i.e.,

$$B_c^{\perp} = \frac{\Phi_0}{2\pi\xi^2}(1 - T/T_c) \tag{1}$$

and

$$B_c^{\parallel} = \frac{\Phi_0\sqrt{12}}{2\pi\xi d}(1 - T/T_c)^{1/2}. \tag{2}$$

From the extrapolation of the critical magnetic fields at $T = 0$ K, we extracted the in-plane coherence length $\xi = \sqrt{\frac{\Phi_0}{2\pi B_{c,0\ K}^{\perp}}} \approx 60$ nm and the thickness of the superconducting layer $d = \frac{\Phi_0\sqrt{3}}{\pi\xi B_{c,0\ K}^{\parallel}} \approx 10$ nm. The fact that the superconducting coherence length is larger than the estimated thickness is consistent with the 2D character of superconductivity.

In fact, $B_c^{\parallel}$ can seemingly go far beyond the Pauli paramagnetic limit, which gives an upper bound for the critical magnetic field resulting from field-induced pair breaking [26,27]. For weak coupling Bardeen-Cooper-Schrieffer (BCS) superconductors, this value is given by

$$B_c^{P} \approx 1.76 k_B T_c / \sqrt{2}\mu_B, \tag{3}$$

where k_B is the Boltzmann's constant and μ_B is the Bohr magneton.

Violation of the paramagnetic limit has been observed in (001)- and (110)-oriented LAO/STO interfaces [22,28,29], as well as in other STO-based superconductors [30]. In these systems, the paramagnetic limit is exceeded by a factor of approximately 3–5. In our case, we find $B_c^{P} \approx 200$ mT, which results in a violation of the Pauli paramagnetic limit by a factor of 10, since $B_{c,0\ K}^{\parallel} \approx 2000$ mT. As a matter of fact, the violation is already present at temperatures very close to T_c, as shown by the dashed line in Fig. 3(b). The enhancement of $B_c^{\parallel}$ well beyond the BCS prediction has been reported in superconductors which display strong spin-orbit effects [31–33]. These are expected to cause randomization of electron spins, and thus result in suppression of the effect of spin paramagnetism [34]. Indeed, we have confirmed the
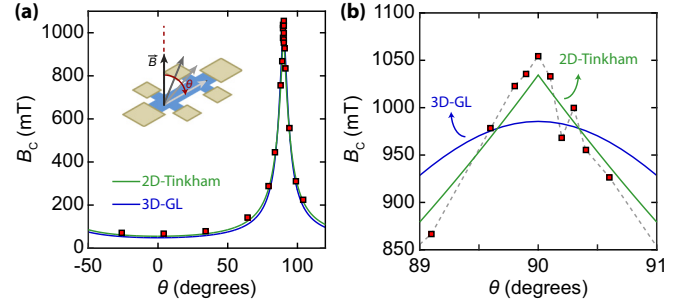
presence of strong spin-orbit fluctuations in the system by magnetotransport measurements (see Supplemental Material), suggesting that spin-orbit coupling plays an important role in the violation of the Pauli paramagnetic limit.

To further investigate the dimensionality of the superconducting layer, we have studied the angular dependence of the critical magnetic field at $T = 82$ mK. Figure 4(a) shows the critical magnetic field as a function of the angle θ, defined between the magnetic field vector and the normal to the surface. The data was fitted with the 2D Tinkham formula (green curve) and the three-dimensional (3D) anisotropic Ginzburg-Landau model (blue curve), given by

$$\frac{B_c^{\theta}|\cos(\theta)|}{B_c^{\perp}} + \left(\frac{B_c^{\theta}\sin(\theta)}{B_c^{\parallel}}\right)^2 = 1 \tag{4}$$

and

$$\left(\frac{B_c^{\theta}\cos(\theta)}{B_c^{\perp}}\right)^2 + \left(\frac{B_c^{\theta}\sin(\theta)}{B_c^{\parallel}}\right)^2 = 1, \tag{5}$$

respectively.

For the overall range, the data seems to be well described by both models. However, a closer look at the region around $\theta = 90°$ in Fig. 4(b) reveals a clear difference between the two models: the 3D model yields a rounded maximum when the magnetic field vector is completely in plane, while the observed cusp-shaped peak can only be well captured by the 2D model.

In summary, by means of systematic (magneto)transport measurements we have demonstrated that the electrons hosted at the (111)LAO/STO interface condense into a superconducting ground state with $T_c \approx 117$ mK. The estimated thickness of the 2D superconducting layer is approximately 10 nm, very similar to the one usually reported for (001)-oriented interfaces. The $V(I)$ characteristics are consistent with a BKT transition, and the two-dimensional character of the superconducting layer was further corroborated by the angular dependence of the critical magnetic field. The Pauli paramagnetic limit is exceeded by a factor of 10, indicating strong spin-orbit coupling in the system. In view of the differences between the symmetries, electronic structure, and orbital ordering of the confined states at the (001)- and (111)-oriented LAO/STO interfaces, further investigation of the latter can

FIG. 4. (a) Angular dependence of the critical magnetic field B_c, where θ is the angle between the magnetic field and the surface normal. Green line: fit to the 2D Tinkham formula. Blue line: fit to the 3D anisotropic Ginzburg-Landau model. (b) Magnified view of the region around $\theta = 90°$.

extend the current understanding of the link between orbital symmetry and superconductivity at LAO/STO interfaces.

[1] H. Hwang, Y. Iwasa, M. Kawasaki, B. Keimer, N. Nagaosa, and Y. Tokura, Nat. Mater. **11**, 103 (2012).

[2] A. Ohtomo and H. Hwang, Nature (London) **427**, 423 (2004).

[3] S. Thiel, G. Hammerl, A. Schmehl, C. Schneider, and J. Mannhart, Science **313**, 1942 (2006).

[4] C. Cen, S. Thiel, G. Hammerl, C. Schneider, K. Andersen, C. Hellberg, J. Mannhart, and J. Levy, Nat. Mater. **7**, 298 (2008).

[5] A. D. Caviglia, M. Gabay, S. Gariglio, N. Reyren, C. Cancellieri, and J.-M. Triscone, Phys. Rev. Lett. **104**, 126803 (2010).

[6] N. Reyren, S. Thiel, A. Caviglia, L. F. Kourkoutis, G. Hammerl, C. Richter, C. Schneider, T. Kopp, A.-S. Rüetschi, D. Jaccard, M. Gabay, D. Muller, J.-M. Triscone, and J. Mannhart, Science **317**, 1196 (2007).

[7] J. Bert, B. Kalisky, C. Bell, M. Kim, Y. Hikita, H. Hwang, and K. Moler, Nat. Phys. **7**, 767 (2011).

[8] L. Li, C. Richter, J. Mannhart, and R. Ashoori, Nat. Phys. **7**, 762 (2011).

[9] G. Herranz, G. Singh, N. Bergeal, A. Jouan, J. Lesueur, J. Gázquez, M. Varela, M. Scigaj, N. Dix, F. Sánchez, and J. Fontcuberta, Nat. Commun. **6**, 6028 (2015).

[10] D. Xiao, W. Zhu, Y. Ran, N. Nagaosa, and S. Okamoto, Nat. Commun. **2**, 596 (2011).

[11] G. Herranz, F. Sánchez, N. Dix, M. Scigaj, and J. Fontcuberta, Sci. Rep. **2**, 758 (2012).

[12] T. C. Rödel, C. Bareille, F. Fortuna, C. Baumier, F. Bertran, P. L. Fèvre, M. Gabay, O. H. Cubelos, M. J. Rozenberg, T. Maroutian, P. Lecoeur, and A. F. Santander-Syro, Phys. Rev. Appl. **1**, 051002 (2014).

[13] S. McKeown Walker, A. de la Torre, F. Y. Bruno, A. Tamai, T. K. Kim, M. Hoesch, M. Shi, M. S. Bahramy, P. D. C. King, and F. Baumberger, Phys. Rev. Lett. **113**, 177601 (2014).

[14] L. Miao, R. Du, Y. Yin, and Q. Li, Appl. Phys. Lett. **109**, 261604 (2016).

[15] P. K. Rout, I. Agireen, E. Maniv, M. Goldstein, and Y. Dagan, Phys. Rev. B **95**, 241107(R) (2017).

[16] M. S. Scheurer, D. F. Agterberg, and J. Schmalian, npj Quant. Mater. **2**, 9 (2017).

[17] A. Joshua, S. Pecker, J. Ruhman, E. Altman, and S. Ilani, Nat. Commun. **3**, 1129 (2012).

[18] See Supplemental Material at http://link.aps.org/supplemental/10.1103/PhysRevB.96.020504 for a complete description of the fabrication process, details on the determination of the critical magnetic field and estimation of spin-orbit coupling.

[19] S. K. Davis, Z. Huang, K. Han, T. Venkatesan, and V. Chandrasekhar, Adv. Mater. Interfaces **4**, 1600830 (2017).

[20] J. Kosterlitz and D. Thouless, J. Phys. C **5**, L124 (1972).

[21] J. M. Kosterlitz and D. J. Thouless, J. Phys. C **6**, 1181 (1973).

[22] Y.-L. Han, S.-C. Shen, J. You, H.-O. Li, Z.-Z. Luo, C.-J. Li, G.-L. Qu, C.-M. Xiong, R.-F. Dou, L. He, D. Naugle, G.-P. Guo, and J. Nie, Appl. Phys. Lett. **105**, 192603 (2014).

[23] J. A. Bert, K. C. Nowack, B. Kalisky, H. Noad, J. R. Kirtley, C. Bell, H. K. Sato, M. Hosoda, Y. Hikita, H. Y. Hwang, and K. A. Moler, Phys. Rev. B **86**, 060503 (2012).

[24] H. Noad, E. M. Spanton, K. C. Nowack, H. Inoue, M. Kim, T. A. Merz, C. Bell, Y. Hikita, R. Xu, W. Liu *et al.*, Phys. Rev. B **94**, 174516 (2016).

[25] P. G. Baity, X. Shi, Z. Shi, L. Benfatto, and D. Popović, Phys. Rev. B **93**, 024519 (2016).

[26] B. Chandrasekhar, Appl. Phys. Lett. **1**, 7 (1962).

[27] A. Clogston, Phys. Rev. Lett. **9**, 266 (1962).

[28] N. Reyren, S. Gariglio, A. D. Caviglia, D. Jaccard, T. Schneider, and J.-M. Triscone, Appl. Phys. Lett. **94**, 112506 (2009).

[29] M. B. Shalom, M. Sachs, D. Rakhmilevitch, A. Palevski, and Y. Dagan, Phys. Rev. Lett. **104**, 126802 (2010).

[30] M. Kim, Y. Kozuka, C. Bell, Y. Hikita, and H. Y. Hwang, Phys. Rev. B **86**, 085121 (2012).

[31] Y. Lu, T. Takayama, A. F. Bangura, Y. Katsura, D. Hashizume, and H. Takagi, J. Phys. Soc. Jpn. **83**, 023702 (2013).

[32] S. Khim, B. Lee, J. W. Kim, E. S. Choi, G. R. Stewart, and K. H. Kim, Phys. Rev. B **84**, 104502 (2011).

[33] H. J. Gardner, A. Kumar, L. Yu, P. Xiong, M. P. Warusawithana, L. Wang, O. Vafek, and D. G. Schlom, Nat. Phys. **7**, 895 (2011).

[34] K. Maki, Phys. Rev. **148**, 362 (1966).